Progress in Physics of Applied Materials 2 (2022) 1–10

Semnan University

Progress in Physics of Applied Materials

journal homepage: https://ppam.semnan.ac.ir/

# Structural, electrical and optical properties of $SnO_2$: B transparent semiconducting thin films

**A. S. Shamsipoor, M. M. Bagheri Mohagheghi*, E. Mokaripoor**

*School of Physics, Damghan University, Damghan, Iran.*

**ARTICLE INFO**

Article history:
Received: 17 February 2022
Revised: 8 April 2022
Accepted: 26 April 2022

Keywords:
Semiconductor thin films
$SnO_2$
Boron
Spray pyrolysis

**ABSTRACT**

Boron (B) is considered as an important impurity in semiconductor physics and optoelectronic devices, especially to produce p-type silicon (p-Si). In this paper, we investigate the effect of Boron doping on the structural, electrical, optical, and photo-sensitivity properties of tin oxide ($SnO_2$) semiconductor thin films. Boron doped tin oxide ($SnO_2$: B) thin films were deposited on glass substrates at $T_s$=500° C for different atomic concentration of x=[B/Sn] = 0, 0.02, 0.04, 0.08, 0.10, 0.20, 0.30, and 0.50 by spray pyrolysis technique. The results of X-ray diffraction (XRD) analysis show the tetragonal rutile $SnO_2$ structure with orientation along the (211) plane. The films have polycrystalline structure with granular and island-like grains morphology by Field-Emission Electron Microscope (FE-SEM). The $SnO_2$:B films have shown n-type conductivity and decreasing - increasing behavior of electrical resistivity with B-doping for x ≤ 0.04 and x> 0.04, respectively. Also, carrier concentrations were obtained in the order of $10^{18}$-$10^{20}$ $cm^{-3}$. Average optical transmittance of $SnO_2$:B thin films changed in the range of 65% to 87% in the visible region and $SnO_2$:B (x=0.08) sample has highest transmittance. The optical gap of films was obtained in the range of 3.47-3.87 eV. From the photoconductive results, the x=0.50 film has exhibited the most optical sensitivity under light radiation.

## 1. Introduction

Nanostructures and thin films of transparent conductive oxides (TCOs) have been widely used in various applications. The two of the most important of these oxides are fluoride- tin oxide (FTO), and indium- tin oxide (ITO). These oxides have a window of transparency in the visible region (400-760 nm) and high electrical conductivity in the range of $10^5$-$10^6$ $\Omega^{-1}cm^{-1}$. The high conductivity of these films is due to the high density of free carriers and crystal defects, especially oxygen vacancy, and their high transparency is due to their wide band gap about $E_g \geq 3$eV [1-5]. Due to these optical and electrical properties, the TCO materials have been used in transparent electrodes and optoelectronic applications such as thin film solar cells, photoresist, gas sensors, heat reflecting mirrors, organic light-emitting diodes and a variety of solid-state devices. Utmost of TCO materials are n-type semiconductors, but p-type TCO materials are required for the development of solid-state devices and p-n junctions [4-11]. Table 1 presents some of the electrical and structural properties of these oxides such as $SnO_2$ and ZnO [12].

Recently, with the development of nano-science, a lot of attention has been paid to these nanostructures including nanowires, nanosheets, nanolayers, quantum dots, nanofibers, nanotubes, nanoparticles of zinc oxide, and tin oxides.

The $SnO_2$ as the most common TCO, is inexpensive, chemically, and thermally strong stable in different environmental conditions which are important attributes for the fabrication and operation of solar cells[12,13]. The $SnO_2$ has a rutile structure, with the wide band gap of $E_g \approx$ 3.78 eV and behave as an n-type semiconductor. In rutile structure, each tin atom is bonded by six oxygen atoms in an octahedral structure, and each oxygen is linked by three tin atoms as planar. Also, the band structure of $SnO_2$ thin films was calculated by the plane wave model, using the generalized gradient approximation (GGA) from local density functional theory (LDFT)[14,15].

In Table 2, some prepared doped-TCOs thin films are listed[8-11]. The impurities used for each specific application must meet certain requirements for the doping process to be successful, including: ionic radius size, atomic valence, empty electron orbital, the type of lattice structure compatible with the host lattice, and bond energy between the main ion - concentration ion [3-7]. In addition, for the suitable substitution of an impurity at the host lattice sites, the bond energy between ion - ion is very important. For the tin oxide semiconductor with boron impurity, the bond energy and bond length of Sn-O, Sn-Sn, B-B, B-Sn, and B-O

* Corresponding author. Tel.: +989183180323
*E-mail address:* ***bmohagheghi@du.ac.ir***

DOI: **10.22075/ppam.2022.26130.1023**

**Table 1.** Electrochemical properties of the three selected MOS ($TiO_2$, ZnO and $SnO_2$)[12].

| Characterize | $SnO_2$ | $TiO_2$ | ZnO |
|---|---|---|---|
| Crystal structure | Rutile | Rutile, anatase, brookite | Rock-salt, zinc blende, wurtzite |
| Energy band gap (eV) | 3.50–4.0 | 3.0–3.2 | 3.2–3.3 |
| Surface work function (eV) | 4.71–5.33 | 4.5–5.0 | 4.45–5.3 |
| CB energy Min vs. Vacuum | 5 eV | 4.1 eV | 4.0 eV |
| Vacuum CB orbitals | Sn (5s&5p) | Ti (3d) | Zn (3d) & O (2p) |
| Valence band orbitals | O(2p) | O(2p) & Ti (3d) | Zn(3d) |
| Electron mobility ($cm^2$ V $s^{-1}$ ) | 240 | 0.1–4 | Bulk ZnO: 205–300; Nanowire: 1000 |
| Refractive index | 2.0 | 2.5 | 2.0 |
| Electron effective mass ($m^*$) | 0.3 | 9 | 0.26 |
| Hole effective mass ($m^*$) | 12.5 $m_e$ | 2 $m_e$ | 8.5 $m_e$ |
| Dielectric constant | 12.5 | 114 | 8.5 |
| Electron diffusion coefficient ($cm^2$ $s^{-1}$ ) | Nanoparticle film: $6.22 \times 10^{-6}$ | Bulk $TiO_2$ : 0.5; Nanoparticles: $10^{-8}$ –$10^{-4}$ | Bulk ZnO: 5.2; Nanoparticle film: $1.7 \times 10^{-4}$ |

**Table 2**. TCO compounds and dopants.

| TCO | Dopant | Applications | Ref. |
|---|---|---|---|
| $SnO_2$ | Sb, F, As, Nb, Ta, Fe, Cu, Mn, Co | Transparent Electrode, Sensor, solar cells, … | [38] |
| ZnO | Al, Ga, B, In, Y, Sc, F, V, Si, Ge, Ti, Zr, Hf, Mg, As, H | Transparent Electrode Optical absorbance, gas sensor, … | [39] |
| $In_2O_3$ | Sn, Mo, Ta, W, Zr, F, Ge, Nb, Hf, Mg, Al, Cr | Transparent Electrode, gas sensor, | [40] |
| CdO | In, Sn | Transparent Electrode, photoluminescence device | [29] |
| $GaInO_3$ | Sn, Ge | gas sensor, optoelectronic device, solar cells | [40] |
| $CdSb_2O_3$ | Y | gas sensor, optoelectronic device | [1] |

are given in Table 3. It is observed which is possible to form a Sn-B bond due to less dissociation energy.

**Table 3**. Bond dissociation energies in diatomic molecules.

| A-B bond | Sn-Sn | Sn-O | Sn-B | B-B | B-O |
|---|---|---|---|---|---|
| Bond Energy (kJ/mol) | 187 | 528 | 325 | 290 | 809 |
| Bond length (Å) | 2.81 | 2.21 | 2.14 | 1.92 | 1.30 |

If these conditions do not prevail, the addition of impurities will cause disorder of structural lattice and increase electron scattering, and we will not achieve the desired goal. Therefore, the selection of impurity atoms to achieve the desired electrical and optical properties will be of particular importance. In some of these properties, the dependence of the structure to the host- atom lattice and the energy gap changes are extremely important, which limits the choice of impurities. However, determining the type of donor or acceptor atom, energy gap engineering and, energy bond structure in achieving applications in the preparation of transparent semiconductors is the subject of ongoing research[9-13]. The energy band gap of

semiconductor oxides such as $SnO_2$ (3.78 eV) and ZnO (3.27 eV) are in comparison of the other wide band gap oxides [12,14].

The $SnO_2$ thin films were deposited by many methods such as physical and chemical vapor deposition, dip and chemical bath coating, sol-gel and spray pyrolysis [15-20]. Usually, the films prepared by spray pyrolysis have a crystalline structure and high order. The different elements such as $F^{1-}$, $N^{1-}$, $Sb^{5+}$, $Zn^{2+}$ and $In^{3+}$ have been used as donor and acceptor ions for $SnO_2$ thin film[21-29]. Boron is a nonmetallic chemical element with character "B", atomic number of 5 and oxidation states of −5, −1, 0, +1, +2, +3. Chemically pure boron, which is found in small amounts in meteoroids, is not found naturally on Earth. Electronic arrangement of boron is [He] $2s^2$ $2p^1$ with atomic radius 0.23Å [30].

In this work, Boron doping of tin oxide ($SnO_2$: B) thin films were prepared by spray pyrolysis deposition on the glass substrates at $T_s$=500 ˚C. The main purpose and innovation of this work is to study the effect of low and highly boron (B) doping on the electrical, structural, and optical properties of $SnO_2$ thin films such as electron concentration and energy gap for optoelectronic devices application, to which less has been reported.

## 2. Experimental details

### 2.1. Materials

$SnCl_4$,$5H_2O$ (purity ≥ 99.99%, Fluka) and Boric acid ($H_3BO_3$, purity ≥ 99.99%) as source material, HCl (purity ≥ 99.9 %, Merck) as solvent agent, deionized distilled water ($H_2O$) and Ethanol ($CH_3CH_2OH$, purity ≥ 99.9 % Merck) as solvent and washing

Molecular Weight: $SnCl_4$ . $5H_2O$=350.6 gr/mol and $H_3BO_3$= 61.83 gr/mol.

### 2.2. Deposition of $SnO_2$:B thin films

Spray solution is prepared using the 0.095 mol of tin tetrachloride pentahydrate ($SnCl_4.5H_2O$) in 100 ml solution of ethanol alcohol ($C_2H_5OH$) + distilled water (1:1) and droplets of HCl and stirring for 20 min at 40 ˚C. Boron doping were done with dissolving boric acid ($H_3BO_3$) in the 10 cc precursor solution and with various B-concentration i.e., [B/Sn] atomic ratio at values x= 0, 0.02, 0.04, 0.08, 0.10, 0.20, 0.30, and 0.50. Table 4 shows the concentration of solutions in moles at 10 cc of spray solution for each step of spray deposition.

For deposition of films, the glass substrates with area of 7.5×2.5 $cm^2$ and 1mm thickness were used. Before preparing the films, the substrates were cleaned by with wash solution and doubled distilled water and dried with air flow. Filtered compressed air was used as carrier gas with the flow rate of 3 $cm^3$/ min at a pressure of 3 atm. The spray nozzle-to-substrate distance was adjusted to 35 cm. The rate of spray about 5 ml/min was maintained at ~10 min for volume (V)=15 $cm^3$. The normalized deposition temperature was T=500 ˚C for $SnO_2$ and Boron-doing of $SnO_2$ films[24]. The uniform deposition was done by rotating the hot plate with rate of 20 rpm.

### 2.3. Characterization

The structure of the deposited films was investigated by X-ray diffraction (XRD), D8 Advance Bruker system using Cu Kα (λ = 0.15406 nm) radiation. The morphology of the films was observed by Field Emission Scanning Electron Microscopy (FE-SEM, Model: Hitachi S-4160). The optical properties of the films including optical transparency, absorption, and optical gap of the thin films were determined by UV-Vis spectrometer and their electrical properties such as electrical resistivity, and concentration and type of carriers were determined by the Hall effect.

The sheet resistance ($R_S$) of the films measured by two-point probe method with aluminum electrodes on two sides of films. The electrical resistivity ($\rho$) of the films was obtained from the equation 1 (t= thickness of film) [24]:

$$\rho(\Omega.cm) = R_S \times t \quad (1)$$

The Hall effect experiment was performed by a magnetic field (B = 200 mT) to determine the concentration and the type of the majority carriers.

The optical properties were studied in the range of 180–1100 nm using Unico 4802 double beam spectrophotometer system. To study the photoconductivity properties the films, samples were exposed to light radiation with a static power (6000 Lux) at a distance (20 cm) using a tungsten fiber lamp. Then, the electrical resistivity (ρ) of prepared films was recorded under lighting at definite time intervals at room temperature.

**Table 4 .** The concentration of solutions in mole for 10 cc precursor solution. (Molecular Weight: $SnCl_4$ . $5H_2O$=350.6 gr/mol and $H_3BO_3$= 61.83 gr/mol)

| Mole: in 10 cc | x=[B/Sn]=0 | x=0.02 | x=0.04 | x=0.08 | x=0.10 | x=0.20 | x=0.30 | x=0.50 |
|---|---|---|---|---|---|---|---|---|
| Mole of $H_3BO_3$ | 0 | $1.9\times10^{-4}$ | $3.8\times10^{-4}$ | $7.6\times10^{-4}$ | $9.5\times10^{-4}$ | $1.9\times10^{-3}$ | $2.85\times10^{-3}$ | $4.75\times10^{-3}$ |
| Mol of $SnCl_4.5H_2O$ | $9.5\times10^{-3}$ | $9.5\times10^{-3}$ | $9.5\times10^{-3}$ | $9.5\times10^{-3}$ | $9.5\times10^{-3}$ | $9.5\times10^{-3}$ | $9.5\times10^{-3}$ | $9.5\times10^{-3}$ |

## 3.Results and discussion

### 3.1. Structural properties

As shown in figure 1, the $SnO_2$:B thin films with doping concentration from 0 to 50 (at. %) were studied by XRD patterns in the 2θ =20˚-70˚. Regardless of B-concentration, it can be seen that the deposited films are polycrystalline. The XRD spectra matched well with $SnO_2$ phase and space group $P4_2mnm$ according to JCPDS (No. 41-1445). The XRD analysis shows that, all films, regardless of the level of boron concentration, have a polycrystalline phase, with

characteristic peaks of (110), (101), (200), (211), and (301) crystallographic planes correspond to the tin oxide ($SnO_2$) phase. In addition, some unstable phases of SnO and $Sn_2O_3$ are observed and two preferred directions can be seen on (200) and (211) planes, which is the maximum intensity for the B-concentration values of x=[B/Sn] =0.2 and 0.04, respectively. As the boron concentration increases to x = 0.08, the intensity of the peaks increases. However, with the further increase of the B concentration, the intensity of the peaks decreases, which is due to the lattice disorder, in each doping level. From the level x = 0.08 onwards, the lattice becomes completely disordered and at x = 0.50, the structure becomes amorphous. This disorder affects the electrical properties and mobility of the carriers so that the conductivity of the films is gradually reduced [25]. This is consistent with the results in the section on electrical properties. In addition, at high doping levels, the intensity of diffraction peaks changes, especially the unstable phases, which are almost eliminated. For example, intensity of (211) preferred peak, initially is increased up to x= 0.04 of B-concentration and then intensity of (211) decreased with increasing B-concentration. After that, with increasing B-concentration a competition between the intensities of (200) and (110) is formed, as the intensity of (200) was highly grown in x=0.20 of B-concentration. According to the ionic radius $B^{3+}$ (r =0.23 Å) and $Sn^{4+}$ (r= 0.71 Å), in high doping of boron, $B^{3+}$ ions can be replaced in interstitial sites of the $SnO_2$ lattice. The small shift of peaks, including (110), is due to the strain of the lattice and substitution of boron impurity [25, 28]. With further concentration for x> 0.20, intensity of peaks is decreased and goes into amorphous structure, probably because of occupying all the interstitials, decrease of grain size at high doping level and disorder of $SnO_2$ lattice structure.

The crystallite size (D) is calculated using Scherrer's relation [31,32]:

$$D=\frac{0.9\lambda}{\beta\ cos\theta} \quad (2)$$

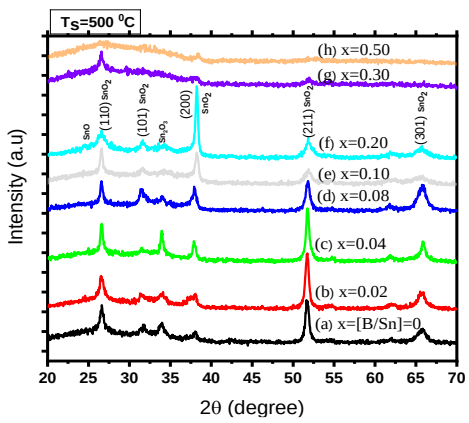


**Fig. 1.** (a) - (h): XRD patterns of Boron-doped $SnO_2$ with various B concentrations (x).

Here, *D* is the crystalline size, β is the peak width of the diffraction line measured at half its maximum intensity (FWHM) (rad), and λ is the X-ray wavelength (1.5406 Å). The structural data, and the identified phases for preferred peak, have been summarized in Table 5. As seen, the average crystallite size is varied with the [B]/[Sn] atomic ratio. It is observed that with increasing the B-concentration as gradually, the crystallite size is increased. The crystalline size of thin films is in range of 15-25 nm.

### *3.2. Morphology of films*

Figs 2. (a)-(h) show the SEM images from surface of $SnO_2$: B thin films. It is shown that the surface morphology of the films was always depend on the B-concentration. The SEM images show that all films with B-doping in crystal lattice from low to high values have an almost uniform structure and an island-like shape with granular morphology. As the doping level increases up to x=0.04, the size of the islands is increased and then decreases as the doping level increases further. In general, increasing boron does not affect the morphology of the layers, but usually at larger sizes the dispersion of the carriers decreases and we expect that the mobility of the carriers will increase and the conductivity of the layers will increase. The particle sizes up to x=0.04 increases with increasing B-concentration. At x=0.08 of B-concentration, more fine polyhedrons nanoparticles are observed. This situation may be related to the reduced preferred peak of (211) at x = 0.08.

At x=0.20 of B-concentration, the grain size increased due to growth of peak (200). Then, as the B-doping is increased further for x> 0.20, size of the spherical and polyhedron nanoparticles again decreases.

### *3.3. Optical properties and optical band gap*

For a transparent semiconductor thin film such as $SnO_2$, the most important quantities are the determination of transparency, absorption and optical gap. Therefore, referring to figure 3, the transmission spectra of the films show that the transparency varies approximately between 65% and 85% for all films. The highest optical transparency is for x = 0.08 and with more increasing boron concentration, the transparency decreases. Indeed, transmittance decreased from T=87% to T=65% with further B-concentration from x=0.08 to x=0.50. The lower transmittance may be attributed to increasing thickness or scattering from film surface. Also, there is a minor shift in the optical absorption edge due to change of band gap. The shift in the absorption edge can be related to increase in carrier concentration and forbidden of low energy transitions [33].

The direct band gap ($E_g$) of the films was found from linear fit of $(\alpha h\nu)^2$ curve versus photon energy (hν) and using the following equation [33]:

$$(\alpha h\nu)^2 = A\ (h\nu - E_g) \quad (3)$$

where α and $E_g$ are the absorption coefficient and the energy gap, respectively, and A is a constant. Fig.4 presents the variation of $(\alpha h\nu)^2$ versus hν (photon energy) for the $SnO_2$: B films. Also, variation of the energy gap and concentration (n) with crystalline size versus the [B]/[Sn] atomic ratio is shown in Fig.5. Here, as the B-concentration increases from x=0 to 0.04, the gap increases from 3.75 to 3.87 and again is reduced with a further increase of up to

0.50 to 3.47. The initial increasing in the gap is attributed to the increase in carrier density and the subsequent decrease is attributed to the decrease in carrier density, as seen Table 6. In fact, the variation of band gap due to doping is a result of the Moss-Burstein (MB) effect, in which the band gap can be presented as $E_g=E_{go}+\Delta E_{MB}$, where $E_{go}$ is the intrinsic band gap and $\Delta E_{MB} = h/2m^* \times (3\pi^2 n_e)^{2/3}$ where m* is the electron effective mass and $n_e$ the electron concentration) [34,35].

With further increase in the B-concentration in the $SnO_2$ films (from 8 at. % B onward) the band gap of films begins to decrease with decrease in carrier concentration (n) revealing Roth effect [36] as it was mentioned in Table 6. As seen in figure 5, Variation of band gap and electron concentration have agreement with each other. From the oscillation of the transmittance spectra, the thickness of the films (t) was determined by using the following equation [37]:

$$t = \frac{\lambda_1 \lambda_2}{2n(\lambda_1 - \lambda_2)} \tag{4}$$

in which, $\lambda_1$ and $\lambda_2$ are the two consecutive peaks in transmission spectra and n is the refractive index of material (n ≈ 2 for $SnO_2$). The thickness of films was changed between 480 nm-820 nm as shown in Table 6. It was observed that the thickness of the film changes with B doping level but does not present trend with increasing B concentration more than x ≥ 10%.

**Table 5.** Summary of the XRD parameters and mean grain size for crystallographic two preferred orientations in various B-concentrations.

| (hkl) | 2θ ($^0$) | Lattice distance(Å) | FWHM ($^0$) | Mean nano-crystal Size (D, nm) | Phase type |
|---|---|---|---|---|---|
| $SnO_2$ | | | | | |
| 110 | 26.68 | 3.3385 | 0.547 | 20.69 | Tetragonal-$SnO_2$ |
| 211 | 51.777 | 1.7642 | 0.53 | 20.69 | Tetragonal-$SnO_2$ |
| $SnO_2$: B (2 at.%) | | | | | |
| 110 | 26.651 | 3.3420 | 0.565 | 19.52 | Tetragonal-$SnO_2$ |
| 211 | 51.771 | 1.7644 | 0.518 | 21.33 | Tetragonal-$SnO_2$ |
| $SnO_2$: B (4 at.%) | | | | | |
| 110 | 26.579 | 3.3510 | 0.338 | 32.24 | Tetragonal-$SnO_2$ |
| 211 | 51.743 | 1.7653 | 0.444 | 24.75 | Tetragonal-$SnO_2$ |
| $SnO_2$: B (8 at.%) | | | | | |
| 110 | 26.567 | 3.3524 | 0.387 | 27.72 | Tetragonal-$SnO_2$ |
| 211 | 51.772 | 1.7643 | 0.58 | 18.99 | Tetragonal-$SnO_2$ |
| $SnO_2$: B (10 at.%) | | | | | |
| 110 | 26.566 | 3.3526 | 0.375 | 28.29 | Tetragonal-$SnO_2$ |
| 200 | 38.226 | 2.3525 | 0.542 | 15.40 | Tetragonal-$SnO_2$ |
| $SnO_2$: B (20 at.%) | | | | | |
| 110 | 26.559 | 3.3534 | 0.833 | 12.71 | Tetragonal-$SnO_2$ |
| 200 | 38.203 | 2.3539 | 0.355 | 23.49 | Tetragonal-$SnO_2$ |
| $SnO_2$:B (30 at.%) | | | | | |
| 110 | 26.559 | 3.3534 | 0.585 | 18 | Tetragonal-$SnO_2$ |
| 211 | 51.92 | 1.7597 | 0.581 | 20.38 | Tetragonal-$SnO_2$ |
| $SnO_2$: B (50 at.%) | | | | | |
| 200 | 38.389 | 2.3429 | 0.415 | 20.69 | Tetragonal-$SnO_2$ |

**Table 6.** The electrical measurement results of the $SnO_2$: B films for various B-concentration.

| x=[B]/[Sn] | Sheet resistance ($R_s$, Ω/□) | Resistivity (Ω.cm) ×$10^{-3}$ | Carrier concentration ($n_e$, $cm^{-3}$ ) | Carrier type (Hall effect) | Energy gap ($E_g$, eV) | Thickness (t, nm) |
|---|---|---|---|---|---|---|
| 0.00 | 60 | 2.92 | $2.5 \times 10^{19}$ | (-) | 3.75 | ~488 |
| 0.02 | 28.8 | 2.11 | $1.5 \times 10^{20}$ | (-) | 3.83 | ~735 |
| 0.04 | 28 | 2.18 | $2.8 \times 10^{20}$ | (-) | 3.87 | ~779 |
| 0.08 | 39.5 | 3.11 | $2.1 \times 10^{20}$ | (-) | 3.85 | ~788 |
| 0.10 | 53.7 | 3.74 | $3.8 \times 10^{19}$ | (-) | 3.73 | ~698 |
| 0.20 | 57.16 | 4.22 | $2.6 \times 10^{19}$ | (-) | 3.70 | ~740 |
| 0.30 | 156.6 | 10.35 | $3.3 \times 10^{18}$ | (-) | 3.49 | ~661 |
| 0.50 | 352.2 | 29.02 | $3.1 \times 10^{18}$ | (-) | 3.47 | ~824 |

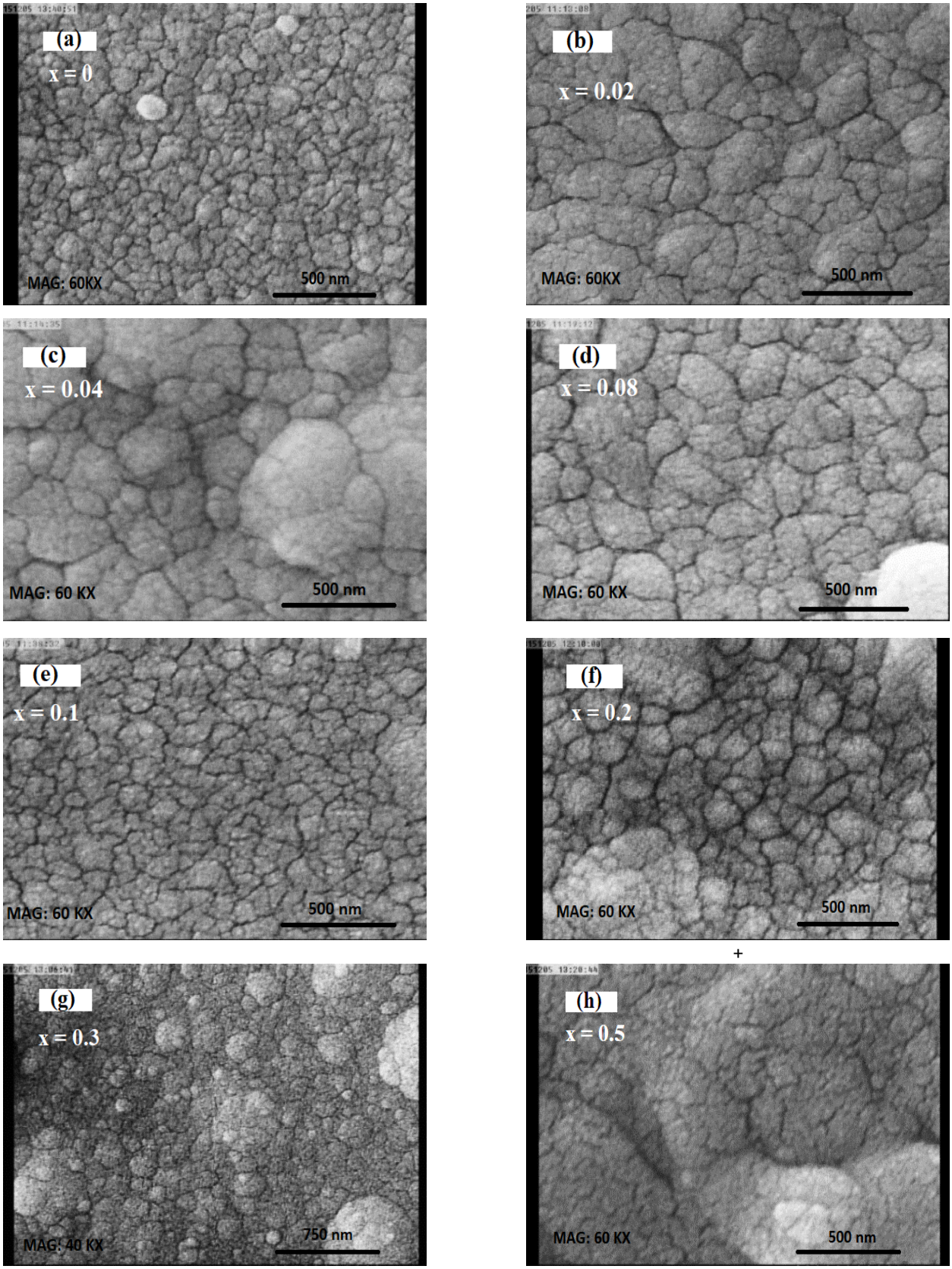


**Fig. 2.** SEM image of $SnO_2$: B thin films with different values of B concentration (x): (a) 0, (b) 0.02, (c) 0.04, (d) 0.08, (e) 0.10, (f) 0.20, (g) 0.30, (h) 0.50.

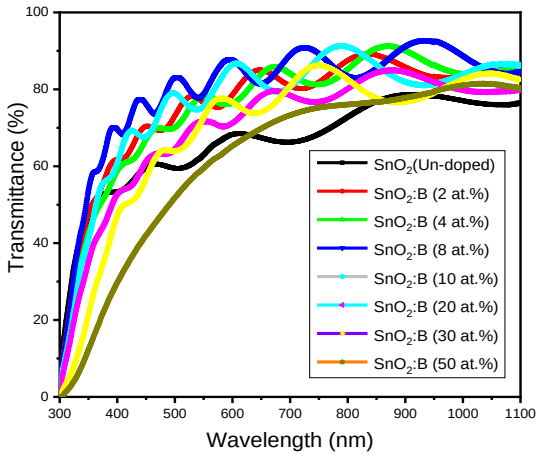


**Fig. 3.** Optical transmittance of $SnO_2$: B films with different values of B concentration (x).

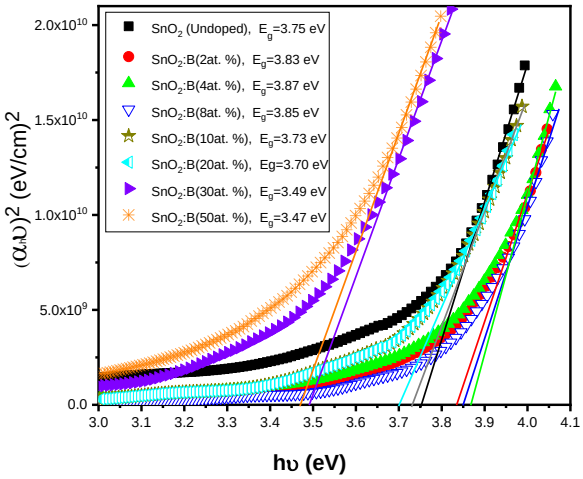


**Fig. 4.** Plots of $(\alpha h\upsilon)^2$ versus hυ for $SnO_2$: B films with different values of B concentration (x).

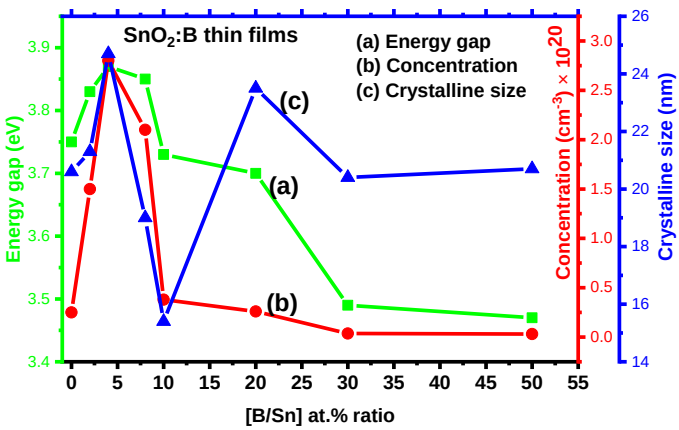


**Fig. 5.** Variation of energy gap ($E_g$) and electron concentration (n)as a function of the [B/Sn] atomic ratio (x).

## 3.4. Electrical properties

The electrical properties of a semiconductor are highly dependent on the density of free carriers (electrons or holes). Usually, donor or acceptor concentration doping is used to increase the conductivity of a semiconductor. The energy level location of concentration is below the conduction band in donor state or above the valance band in acceptor state [38]. Fig.6(a)-(b) shows the location of the donor or acceptor level in band structure of n- type and p-type semiconductor. The donor energy level is obtained from the following equation [39]:

$$E_d = E_c - \frac{e^4\, m_e^*}{2(4\pi\epsilon)^2\, \hbar} \times \frac{1}{n^2} \quad \text{and} \quad n=1,2,\ldots \tag{5}$$

$$E_d = E_c - \frac{e^4\, m_e^*}{2(4\pi\epsilon)^2\, \hbar}\; E_c - 13.6 \left(\frac{m^*}{m_0}\right)\left(\frac{\epsilon_0}{\epsilon}\right)^2 eV \quad \text{for} \quad n=1 \tag{6}$$

Here, $m_e^*$ and $\epsilon$ are effective mass of electron or hole and dielectric constant of semiconductor, respectively. This relation is obtained by calculating the base energy state of electron in a hydrogen atom, which is given to the donors and acceptors level in the lattice of semiconductor with equation 6. The presence of a dopant concentration creates

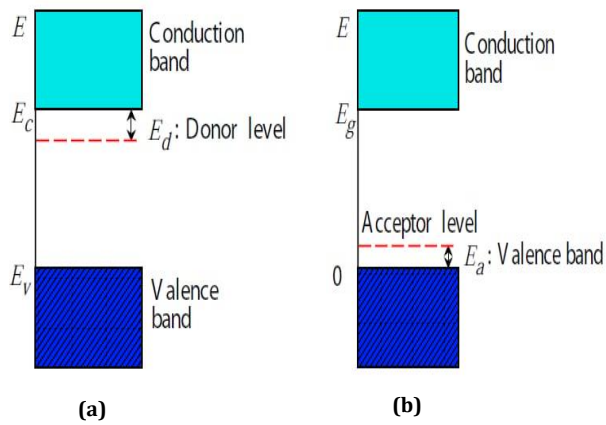


**Fig. 6.** (a), (b): Band structure of n- and p-type semiconductor with donor and acceptor concentration level.

a bound $E_d$ level (or $E_a$) below conduction band (or above valence band) edge). Donor and acceptor energy levels of $SnO_2$ are about 20 meV and 200 meV , respectively. Here, we used $B^{3+}$ ions as acceptor dopant in order to study the effect of $B^{3+}$ on the electrical conductivity.

The results of electrical measurements for all deposited $SnO_2$:B thin films have been summarized in Table 6. Also, variations of resistivity ($\rho$), concentration (n), and energy gap ($E_g$) versus the [B/Sn] atomic ratio ($x$) are shown in figure 7. The sheet resistance (or resistivity) of films has a decreasing-increasing behavior, such as from $R_s$= 60 Ω/□ in x=0 to $R_s$ =28 Ω/□ in x=0.04 and then to $R_s$=57.16 Ω/□ in x=0.20.

The variation of resistivity (or) sheet resistance is related to role of $B^{3+}$ and $Sn^{2+}$ or $Sn^{3+}$ in the ordered sites of $SnO_2$ lattice or interstitial site as donor or acceptor, respectively. For example, $Sb^{5+}$ or $F^{5+}$ ($Al^{3+}$, $Ga^{3+}$, or $B^{3+}$) ions in role of donor (acceptor) create a free electron (free hole) in lattice. As seen in figure 8, substitution of an acceptor impurity such as $B^{3+}$ in $Sn^{4+}$ sites lead to creation of one hole. Boron has only three valence electrons. It can complete its four-fold tetrahedral bonds by taking an electron from an Sn–Sn bond, leaving behind a hole in the

$SnO_2$ band structure. We expected that the boron ions ($B^{3+}$), in role of acceptor, created to create a free hole in $SnO_2$ point of lattice point, but this is not always the case.

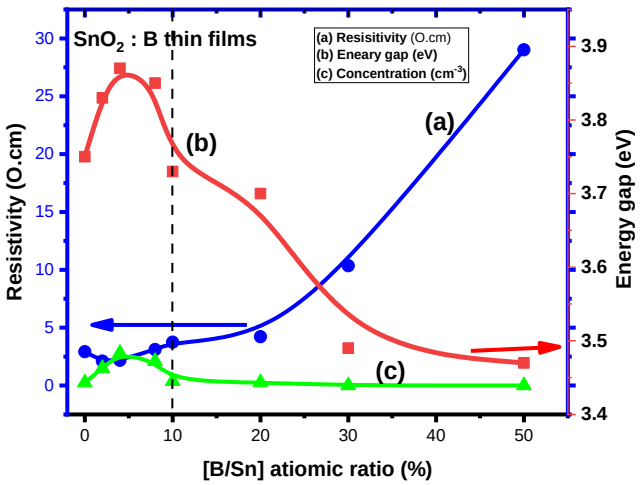


**Fig. 7.** Variation of electrical resistivity, energy gap and electron concentration of SnO2: B thin films.
as function of B concentration concentration (x).

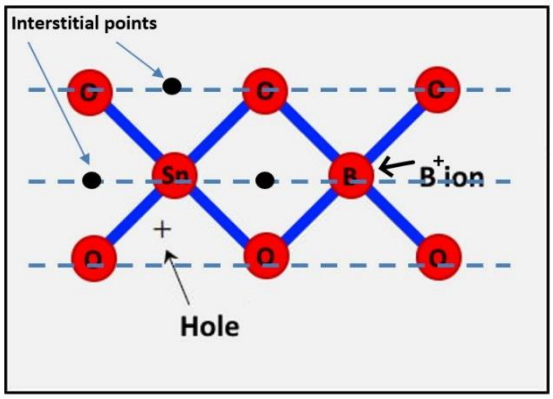


**Fig. 8.** The substitution of $B^{3+}$ concentration as acceptor in $SnO_2$ lattice by taking an electron from an Sn–Sn bond and creation of hole.

This is because of the high mobility and very small ionic radius of $B^{+3}$(r = 0.23Å) with light atomic mass of 10.81 amu in comparison with $Sn^{4+}$(r=0.71Å) with heavy atomic mass (118.71 amu). Indeed, as seen in Table 6 and Fig.2, after x=[B/Sn] > 0.1, the B/$SnO_2$ structures became amorphous and the $SnO_2$ is converted into SnO and $Sn_2O_3$ with valence states of $Sn^{2+}$ and $Sn^{3+}$. Therefore, n-to-p transition is not occurred and type of carrier is negative (-) for all of the films. In addition, $B_2O_3$ is a glass former, which can be formed in lattice, so it is very difficult to break its bonds into a substitute to act as n and p dopants. Consequently, $B^{+3}$ ions do not have the substitution power of $Sn^{+4}$ ions and occupy the interstitial sites of the $SnO_2$ lattice and B-doped films are n-type semiconductor.

The majority carrier concentration was obtained using the following equation by the Hall effect measurements [30]:

$$n = \frac{IB}{qVHt} \quad (7)$$

In this relation, B, I, t, q, and $V_H$ are the magnetic field, current, thickness, electron charge, and Hall voltage, respectively. Table 6 also represents the carrier concentration (n) of the $SnO_2$: B thin film for different B-concentration. The carrier concentration for the film deposited with various B-concentration is in order of $10^{18}$-$10^{20}$cm$^{-3}$ and with increasing the B-concentration up to x=0.04 reach to maximum value, 2.8 ×$10^{20}$ cm$^{-3}$ and then decreased to 3.1×$10^{18}$ cm$^{-3}$ for x=0.50 B-concentration.

### *3.4. Photoconductive and optical response properties*

If we consider a thin film of semiconductor with a direct gap ($E_g$), and valence and conduction bands, when the semiconductor is irradiated with light with hυ ≥ $E_g$ , the phenomenon of optical absorption occurs, so that an electron transmits from the valence band to the conduction band. This process is photoconductive effect, and the result is the production of a free carrier (electron or hole). Due to light absorption, the density of carriers and electrical conductivity increase [39,40]. In other words, this property is used to study the properties of optical sensing as a functional component for electronic eyes, or invisible recognition tools. Photoconductivity changes are measured with an important parameter of optical response (S) i.e., changes in electrical resistance (surface or volume) with light radiation relative to the initial resistance ($R_0$) of the film in absence of light (S=ΔR/R). If the slope of the electrical resistance changes in the presence of light radiation is higher, the sensing property will be higher. Accordingly, the electrical resistance of the layers under light irradiation was measured at equal intervals. The variation of the sheet resistance of the films (ΔR/R) versus radiation time and B-concentration is shown in Figure 9.

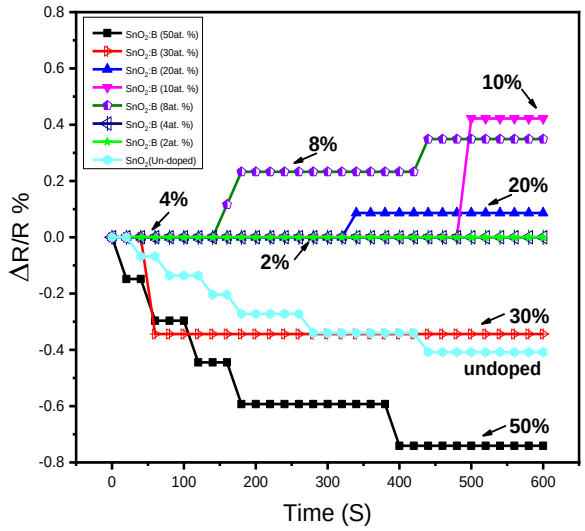


**Fig. 9.** The relative change of sheet resistance (ΔR) versus exposure time for $SnO_2$: B films with different values of B concentration (x).

As seen, the photoconductivity of the films is not changed relatively in low concentration (up to x=0.04) with increasing radiation time. But, in high B-concentration (x > 0.04), the sheet resistance of $SnO_2$:B films is increased. This effect relates to the increase in disorder and amorphous structure of the films at high B-concentration level,

especially at x=0.50 of B-concentration. In x≥ 30, because there are many crystal defects and voids in the $SnO_2$ lattice with the absorption of optical energy, the transition to the conduction band by the electrons is greatly increased. From the photoconductivity studies, the 50 at. % B-doped $SnO_2$ film exhibits sensitivity most to operational light. Therefore, photoinductive properties of these films can be used in optical switching, optical sensors, and transistor devices [29,40].

## 4. Conclusions

In this paper, we studied the preparation and characterization of undoped $SnO_2$ for low and high_boron concentration of $SnO_2$ thin films. The films were deposited on glass substrates at temperature of $T_s$=500 ˚C using the spray pyrolysis.

Among the important results are as following:

(a) It was seen that the structural properties of the films powerfully depended on the B-concentration level. All of the films exhibited a preferential growth along the (211) and (200) directions corresponding to tetragonal $SnO_2$ phase. In general, an increase in concentration doping reduces the particle size. Most of the structural and electrical changes of the films are in the range 0.04 ≤ x ≤ 0.2.

(b) The spherical and polyhedron nanoparticles are observed in the FE-SEM images.

(c) Electrical properties of the films showed that the minimum of sheet resistance of the films is about 28 Ω/□ in x=0.04. The Hall effect measurements have shown the n- type conductivity for all of the films. The highest carrier concentration of $2.8 \times 10^{20} cm^{-3}$ was found for the film deposited with x=0.04.

(d) $B^{3+}$ (or $B^{3-}$) ions can be replaced both in the $Sn^{4+}$ (or $O^{2-}$) and in the interstitial positions in the $SnO_2$ lattice and there is always a competition between them.

(e) Average optical transmittance of $SnO_2$:B thin films changed in the range of 65% to 87% in the visible region and x=0.08 exhibited the highest optical transparency in the visible region. Also, an increase in B-doping leads to a reduction in the energy gap due to increasing the electron concentration.

(f) Photoconductivity and optical response studies showed, the B-doped $SnO_2$ thin films exhibited low sensitivity to incident light up to x=0.04. But, for x> 0.04, changes in conductivity are comparable to radiant light, both positively and negatively. Amongst of B-doped $SnO_2$ films, highest photoconductivity related to the x=0.50.

## References


[1] Afre, Rakesh A., Nallin Sharma, Maheshwar Sharon, and Madhuri Sharon. "Transparent conducting oxide films for various applications: A review." Reviews on advanced materials science 53(1) (2018) 79-89.

[2] Exarhos, G.J. and Zhou, X.D., 2007. Discovery-based design of transparent conducting oxide films. Thin solid films, 515(18) 7025-7052.

[3] Ginley, David S., and John D. Perkins. "Transparent conductors." In Handbook of transparent conductors, pp. 1-25. Springer, Boston, MA, 2011.

[4] Kim, Tae Youn, Jeong Woo Lee, Won Seo Park, Seong Kee Park, Ki Yong Kim, In Byeong Kang, and Jae Min Myoung. "Development of transparent conductive oxide for thin-film silicon solar cells." Journal of the Korean Physical Society 56,(2) (2010) 571-575.

[5] Atay FE, DEMIR M, Kose S, Bilgin Vİ, Akyuz I. Some physical properties of ultrasonically sprayed tin oxide films: the effect of the substrate temperature. Journal of optoelectronics and advanced materials.9(7) (2007).

[6] El Akkad, Fikry, and Tressia AP Paulose. "Optical transitions and point defects in F: SnO2 films: Effect of annealing." Applied surface science 295 (2014) 8-17.

[7] Sancakoglu, Orkut. "Technological Background and Properties of Thin Film Semiconductors." In 21st Century Surface Science-a Handbook. IntechOpen, 2020.

[8] Sathishkumar, M., and S. Geethalakshmi. Enhanced photocatalytic and antibacterial activity of Cu: SnO2 nanoparticles synthesized by microwave assisted method. Materials Today: Proceedings 20 (2020) 54-63.

[9] Miranda, Héctor, and Eleicer Ching-Prado. "Physical Properties of Semiconductor TCO-SnO2: F Thin Film." In 2019 7th International Engineering, Sciences and Technology Conference (IESTEC).IEEE. (2019)103-108.

[10] Ching-Prado, E., A. Watson, and H. Miranda. "Optical and electrical properties of fluorine doped tin oxide thin film." Journal of Materials Science: Materials in Electronics 29(18) (2018) 15299-15306.

[11] Amiri, Iraj Sadegh, and Mahdi Ariannejad. Solar Energy-Based Semiconductors: Working Functions and Mechanisms. In Introducing CTS (Copper-Tin-Sulphide) as a Solar Cell by Using Solar Cell Capacitance Simulator (SCAPS), Springer, Cham, (2019)15-35.

[12] Wali, Qamar, Azhar Fakharuddin, and Rajan Jose. Tin oxide as a photoanode for dye-sensitised solar cells: current progress and future challenges. Journal of Power Sources 293 (2015)1039-1052.

[13] Rajput, Rekha B., and Rohidas B. Kale. Hydro/solvothermally synthesized visible light driven modified SnO2 heterostructure as a photocatalyst for water remediation: A review. Environmental Advances 5 (2021)100081.

[14] Chen, Yichuan, Qi Meng, Linrui Zhang, Changbao Han, Hongli Gao, Yongzhe Zhang, and Hui Yan. SnO2-based electron transporting layer materials for perovskite solar cells: A review of recent progress. Journal of energy chemistry 35 (2019)144-167.

[15] Maleki, M., and S. M. Rozati. An economic CVD technique for pure SnO2 thin films deposition: Temperature effects. Bulletin of Materials Science 36(2),(2013) 217-221.

[16] Oktasendra, Fandi, Rahmat Hidayat, and Rizky Indra Utama. Effects of interface state density on the carrier transport and performance of metal-insulator-semiconductor (MIS) type thin film solar cells. In Journal of Physics: Conference Series,1481(1), IOP Publishing (2020) 012005.

[17] Arularasu, M. V., M. Anbarasu, S. Poovaragan, R. Sundaram, K. Kanimozhi, C. Maria Magdalane, K. Kaviyarasu et al. Structural, optical, morphological and microbial studies on SnO2 nanoparticles prepared by co-precipitation method. Journal of nanoscience and nanotechnology 18(5),(2018) 3511-3517.

[18] Murakami, K., Nakajima, K. and Kaneko, S., Initial growth of SnO2 thin film on the glass substrate deposited by the spray pyrolysis technique. Thin Solid Films, 515(24),(2007) 8632-8636

[19] Elangovan, E., and K. Ramamurthi. Studies on micro-structural and electrical properties of spray-deposited fluorine-doped tin oxide thin films from low-cost precursor. Thin solid films 476 (2)(2005) 231-236.

[20] Taniguchi, I., D. Song, and M. Wakihara. Electrochemical properties of LiM1/6Mn11/6O4 (M= Mn, Co, Al and Ni) as cathode materials for Li-ion batteries prepared by ultrasonic spray pyrolysis method. Journal of power Sources 109(2) (2002) 333-339.

[21] Kaviyarasu, K., Prem Anand Devarajan, S. Stanly John Xavier, S. Augustine Thomas, and S. Selvakumar. One pot synthesis and characterization of cesium doped SnO2 nanocrystals via a hydrothermal process. Journal of Materials Science & Technology 28 (1), (2012)15-20.

[22] Sánchez-García, M. Alberto, Arturo Maldonado, Luis Castañeda, Rutilo Silva-González, and María de la Luz Olvera. Characteristics of SnO2: F thin films deposited by ultrasonic spray pyrolysis: effect of water content in solution and substrate temperature. Materials Sciences and Applications, 3(10) (2012) 690-696.

[23] Geraldo, Viviany, Luis Vicente de Andrade Scalvi, Evandro Augusto de Morais, Celso Valentim Santilli, and Sandra Helena Pulcinelli. "Sb doping effects and oxygen adsorption in SnO2 thin films deposited via sol-gel." Materials Research, 6 (2003) 451-456.

[24] Zhang, B., Tian, Y., Zhang, J.X. and Cai, W., The studies on the role of fluorine in SnO2: F films prepared by spray pyrolysis with SnCl4. Journal of Optoelectronics and Advanced Materials, 13(1),(2011) 89-93.

[25] M. M. Bagheri-Mohagheghi, N. Shahtahmasebi, M. R. Alinejad, A. Youssefi, and M. Shokooh-Saremi. Fe-doped SnO2 transparent semi-conducting thin films deposited by spray pyrolysis technique: Thermoelectric and p-type conductivity properties. Solid State Sciences 11(1),(2009) 233-239.

[26] Turgut, G., Sonmez, E., Aydın, S., Dilber, R., & Turgut, U. The effect of Mo and F double doping on structural, morphological, electrical and optical properties of spray deposited SnO2 thin films. Ceramics International, 40(8), (2014)12891-12898.

[27] Doyan, Aris, Susilawati, and Yanika Diah Imawanti. Synthesis and Characterization of SnO2 thin layer with a doping Aluminum is deposited on Quartz Substrates. In AIP Conference Proceedings, 1801(1)(2017) 020005.

[28] Patil, G. E., D. D. Kajale, S. D. Shinde, V. G. Wagh, V. B. Gaikwad, and G. H. Jain. Synthesis of Cu-doped SnO 2 thin films by spray pyrolysis for gas sensor application. In Advancement in Sensing Technology,(2013) 299-311. Springer, Berlin, Heidelberg.

[29] Dive, A., Varley, J. and Banerjee, S., In2O3-Ga2O3 Alloys as Potential Buffer Layers in CdTe Thin-Film Solar Cells. Physical Review Applied, 15(3),(2021) 034028.

[30] Braunschweig, Holger, Rian D. Dewhurst, Kai Hammond, Jan Mies, Krzysztof Radacki, and Alfredo Vargas. Ambient-temperature isolation of a compound with a boron-boron triple bond. Science 336 (6087), (2012) 1420-1422.

[31] Thomas, Boben, Skariah Benoy, and K. K. Radha. Influence of Cs doping in spray deposited SnO2 thin films for LPG sensors. Sensors and Actuators B: Chemical 133 (2),(2008) 404-413.

[32] Lee, W.Y., Lee, H., Ha, S., Lee, C., Bae, J.H., Kang, I.M. and Jang, J., 2020. Improved negative bias stability of sol–gel processed Ti-doped SnO2 thin-film transistors. Semiconductor Science and Technology, 35(11), (2020)115023.

[33] Girtan, M., Rusu, G.I., Rusu, G.G. and Gurlui, S., Influence of oxidation conditions on the properties of indium oxide thin films. Applied surface science, 162 (2000) 492-498.

[34] Burstein, E., Anomalous optical absorption limit in InSb. Physical review, 93(3),(1954) 632.

[35] Zinchenko, T., Pecherskaya, E., & Artamonov, D. The properties study of transparent conductive oxides (TCO) of tin dioxide (ATO) doped by antimony obtained by spray pyrolysis. AIMS Materials Science, 6(2), (2019) 276-287.

[36] Khan, A. and Rahman, F., Study of microstructural and optical properties of nanocrystalline indium oxide: A transparent conducting oxide (TCO). In AIP Conference Proceedings, 2115(1),(2019) 030091. AIP Publishing LLC.

[37] Kumar, S., Sharma, R., Gupta, A., Tyagi, A., Singh, P., Kumar, A. and Kumar, V., Recent insights into SnO 2-based engineered nanoparticles for sustainable H2 generation and remediation of pesticides. New Journal of Chemistry, 46(9),(2022) 4014-4048.

[38] Türkyılmaz, Şenay Şen, Nuray Güy, and Mahmut Özacar. Photocatalytic efficiencies of Ni, Mn, Fe and Ag doped ZnO nanostructures synthesized by hydrothermal method: The synergistic/antagonistic effect between ZnO and metals. Journal of Photochemistry and Photobiology A: Chemistry 341 (2017) 39-50.

[39] Mishra, Umesh K., and Jasprit Singh. Semiconductor device physics and design.83. Dordrecht: Springer, 2008.

[40] Zhu, Xinxu, Yijie Li, Hongchao Zhang, Longfei Song, Hongliang Zu, Yuanbin Qin, Lei Liu, Ying Li, and Fengyun Wang. High-performance field effect transistors based on large ratio metal (Al, Ga, Cr) doped In2O3 nanofibers. Journal of Alloys and Compounds. 830 (2020)154578.